PAN ARCHIVES OF ACOUSTICS
Vol. **42**, No. 1, pp. 93–104 (2017)

DOI: 10.1515/aoa-2017-0010

Optimized Driver Placement for Array-Driven Flat-Panel Loudspeakers

David A. ANDERSON, Michael C. HEILEMANN, Mark F. BOCKO

Department of Electrical and Computer Engineering
University of Rochester
526 Computer Studies Bldg. Rochester, NY, 14627 USA; e-mail: dander22@ur.rochester.edu

(*received June 27, 2016; accepted November 4, 2016*)

The recently demonstrated 'modal crossover network' method for flat panel loudspeaker tuning employs an array of force drivers to selectively excite one or more panel bending modes from a spectrum of panel bending modes. A regularly spaced grid of drivers is a logical configuration for a two-dimensional driver array, and although this can be effective for exciting multiple panel modes it will not necessarily exhibit strong coupling to all of the modes within a given band of frequencies. In this paper a method is described to find optimal force driver array layouts to enable control of all the panel bending modes within a given frequency band. The optimization is carried out both for dynamic force actuators, treated as point forces, and for piezoelectric patch actuators. The optimized array layouts achieve similar maximum mode coupling efficiencies in comparison with regularly spaced driver arrays; however, in the optimized arrays all of the modes within a specified frequency band may be independently addressed, which is important for achieving a desired loudspeaker frequency response. Experiments on flat panel loudspeakers with optimized force actuator array layouts show that each of the panel modes within a selected frequency band may be addressed independently and that the inter-modal crosstalk is typically −30 dB or less with non-ideal drivers.

Keywords: loudspeaker; array; crossover network; spatial sampling.

1. Introduction

Flat-panel loudspeakers that generate sound via the excitation of bending mode vibrations of a plate can be thin and lightweight in comparison with traditional loudspeaker designs, which gives them an advantage in applications where form factor and weight are critical design constraints. They can also be electrically efficient by using compact, low power force actuators to excite the sound-radiating panel bending vibrations. Designs that employ one (or a small number) of actuators positioned on a panel to couple to the greatest number of panel bending modes have become known as Distributed-Mode Loudspeakers (DMLs) (Bank, Harris, 1998). It has proven difficult to achieve a flat frequency response at low frequencies with DMLs due to the presence of isolated low frequency panel bending modes. There are also large differences in the half-space radiation patterns of the various panel bending modes so achieving a flat low frequency acoustic response with spatial uniformity is especially difficult (Anderson, Bocko, 2015). The Modal Crossover Network (MXN) method was proposed as a way to overcome these problems (Anderson, Bocko, 2016a). In this approach an array of force drivers can be employed to excite a selected panel mode, and importantly, to not excite other panel modes. Typically, the lowest bending mode of a panel is employed. For a rectangular panel with simply supported edges this corresponds to the mode with maximum displacement at the panel center and decreasing to zero at the panel edges, the so-called $(1,1)$ mode. In this case the panel behaves effectively as a large pistonic loudspeaker within a given frequency band.

Depending upon the dimensions and thickness of a panel there may be thousands of panel bending modes within the audio frequency band (20 Hz – 20 kHz). It can be shown that the number of panel modes that are controllable by a given force driver array is only equal to the number of drivers in the array; i.e., the number of modes that can be controlled independently is equal to the number of degrees of freedom of the array (Anderson, Bocko, 2016a). This has the consequence that there will inevitably be higher-order panel modes that will be excited inadvertently – a form of aliasing (Fuller *et al.*, 1996). The MXN method

is designed to control all of the panel modes that lie within a specified frequency band (typically low-pass) with any aliased modes falling above the selected frequency band. It is not necessary to resort to the use of driver arrays and the MXN method to achieve flat frequency response when the low frequency panel bending modes are highly damped ($Q < 1$). However, when a panel exhibits isolated, lightly damped modes ($Q > 1$), the MXN method enables a flatter frequency response to be achieved throughout a low-pass frequency band; the extent of the band being determined by the distribution of panel modes and the number of force actuators in the array. At higher frequencies, where the number of overlapping panel modes activated at any specific frequency increases (Rabbiolo *et al.*, 2004), the vibrational response of a panel is roughly localized to the vicinity of a driver, so each effectively serves as a high-frequency tweeter (Anderson, Bocko, 2016b).

There has been previous research on the optimal driver placement for multi-modal control of complex structures, usually with the goal of actively damping structural vibrations caused by external forces (Porter, Crossley, 1972; Demetriou, 2000). Our work is focused on the case in which a structure is intentionally driven by a broad-band audio signal and the goal is to achieve even response of the structure over the defined frequency band. Since the actuating signal is completely known ahead of time, sensing and feedback is not needed, which simplifies the implementation considerably. Sampling theory can be employed to infer the driver array design required to address each of a given set of panel modes, however, determining the optimized driver locations for such an array is not intuitive so an optimization technique based on energy coupling between actuators and modes has been developed to determine optimal array layouts.

In the second section we present background material on panel modes, modal coupling factors, and mode coupling efficiency. In the third section we describe the algorithm used to determine the optimal locations of point force actuators for a given set of panel modes and several examples of arrays generated using the optimization technique are given. The fourth section presents results using the same optimization technique for piezoelectric bending mode actuators and in the final section experimental results from a prototype loudspeaker built using an optimized array of dynamic force actuators are reported.

2. Flat panel loudspeakers

Flat Panel Loudspeakers radiate acoustic energy by exciting the bending-mode vibrations of a plate with externally applied forces, usually either from voice-coil actuators or piezoelectric bending elements. The classical plate equation, given in Eq. (1) for a plate with dimensions L_x by L_y, relates the applied pressure distribution on the plate, $p(x, y, t)$, to the spatially distributed out-of-plane displacement of the panel, $u(x, y, t)$, where (x, y) represents any point on the panel and t is time. The notation $\ddot{u}(x, y, t)$ represents the second temporal derivative of $u(x, y, t)$.

$$D\nabla^4 u(x, y, t) + \rho h\ddot{u}(x, y, t) = p(x, y, t). \tag{1}$$

In the above equation, D is the bending stiffness of the panel, ρ is the density of the panel material, and h is the panel thickness.

Solutions of Eq. (1) are simplified when the panel displacement is represented as a sum of individual resonant modes (Fuller *et al.*, 1996). The left side of Eq. (1) can be broken into an infinite sum of resonant modes with index r, each with time-dependent amplitude $u_r(t)$, while the force on the right side can be decomposed into a Fourier series for each mode shape such that

$$\sum_{r=1}^{\infty}\left[D\Psi_r^2 u_r(t) + \rho h\ddot{u}_r(t) = \frac{4f_r(t)}{L_x L_y}\right], \tag{2}$$

where

$$\Psi_r = \left(\frac{m_r\pi}{L_x}\right)^2 + \left(\frac{n_r\pi}{L_y}\right)^2 \tag{3}$$

and

$$p(x, y, t) = \sum_{r=1}^{\infty}\frac{4f_r(t)}{L_x L_y}H_r(x, y) \tag{4}$$

with (m_r, n_r) representing the indices of the r-th mode in the x and y directions respectively and $H_r(x, y)$ representing the shape of the r-th mode, which will be explained in more detail below.

The factors $f_r(t)$ represent the contribution of the externally applied force on the r-th panel mode. For N individual drivers at locations (x_i, y_i) this force is given as

$$f_r(t) = \sum_{i=1}^{N}\alpha_r(x_i, y_i)d_i(t), \tag{5}$$

where d_i(t) is the force of the i-th actuator. The effective force of a given actuator on any selected mode is given by the 'coupling factor', $\alpha_r(x, y)$. If the force is applied at a node of a given mode it will not excite that mode regardless of the magnitude of the applied force. Conversely, a force applied at an anti-node of a given mode will drive the mode with maximum efficiency. For a simply supported plate the mode shapes are simple sinusoidal functions so the coupling factor of a driver located at $(x_i,\, y_i)$ to mode r is given as

$$\begin{aligned}\alpha_r(x_i, y_i) &= H_r(x_i, y_i)\\ &= \sin\left(\frac{m_r\pi}{L_x}x_i\right)\sin\left(\frac{n_r\pi}{L_y}y_i\right).\end{aligned} \tag{6}$$

Note that, in the case of forces localized as delta functions, the α factors are equal to the spatial shape function $H_r(x,y)$ at the force location. In the case of more spatially complex drivers, such as the piezoelectric actuators studied in Sec. 4, this will not be the case.

If multiple forces are acting on the plate, the net force on each mode is defined as a sum of each driver force, weighted by their respective coupling factors. This can be represented as a matrix that relates modal forces to driver forces, as shown in Eqs. (7)–(9). $\mathbf{F}$ is an array of R modal forces, $\mathbf{D}$ is an array of N driver forces, and $\mathbf{G}$ is the matrix of coupling factors relating the two. For simplicity, the terms here have not been written as a function of time like they had been in Eq. (5).

$$\mathbf{F} = \begin{bmatrix} f_1 \\ f_2 \\ \vdots \\ f_R \end{bmatrix}, \qquad \mathbf{D} = \begin{bmatrix} d_1 \\ d_2 \\ \vdots \\ d_N \end{bmatrix}, \tag{7}$$

$$\mathbf{G} = \begin{bmatrix} \alpha_1(x_1,y_1) & \alpha_1(x_2,y_2) & \cdots & \alpha_1(x_N,y_N) \\ \alpha_2(x_1,y_1) & \alpha_2(x_2,y_2) & \cdots & \alpha_2(x_N,y_N) \\ \vdots & \vdots & \vdots & \vdots \\ \alpha_R(x_1,y_1) & \alpha_R(x_2,y_2) & \cdots & \alpha_R(x_N,y_N) \end{bmatrix}, \tag{8}$$

$$\mathbf{F} = \mathbf{G}\mathbf{D}. \tag{9}$$

In a modal crossover network, the modal forces are selected to produce the desired loudspeaker characteristics. The details of the tuning methods are not within the scope of this paper but a more in-depth discussion of modal biasing can be found in the references. The individual driver forces are then determined by means of Eq. (10).

$$\mathbf{D} = \mathbf{G}^{-1}\mathbf{F}. \tag{10}$$

Equation (10) requires that the coupling matrix $\mathbf{G}$ be square and have linearly independent rows to be invertible. Furthermore, we also assume that only the first N modes will be the focus of attention so the $\mathbf{G}$ matrix will be $N \times N$ and the $\mathbf{F}$ matrix will be $N \times 1$. This also implies that by employing N actuators it is possible to control N modes, or $R = N$. Equation (8) then becomes,

$$\mathbf{G} = \begin{bmatrix} \alpha_1(x_1,y_1) & \alpha_1(x_2,y_2) & \cdots & \alpha_1(x_N,y_N) \\ \alpha_2(x_1,y_1) & \alpha_2(x_2,y_2) & \cdots & \alpha_2(x_N,y_N) \\ \vdots & \vdots & \vdots & \vdots \\ \alpha_N(x_1,y_1) & \alpha_N(x_2,y_2) & \cdots & \alpha_N(x_N,y_N) \end{bmatrix} \tag{11}$$

and $\mathbf{F}$ in Eq. (7) becomes,

$$\mathbf{F} = \begin{bmatrix} f_1 \\ f_2 \\ \vdots \\ f_N \end{bmatrix}. \tag{12}$$

Aside from the requirement of row independence, the driver locations can be arbitrary. For a given set of modes, there are many array locations that will result in linearly independent rows for the $\mathbf{G}$ matrix. The specific modes that have strong coupling to an arbitrary array layout will not necessarily fall within the MXN bandwidth, which reduces the effectiveness of the array.

2.1. Frequency-based control regions

The maximum excursion of each plate mode results when the plate is driven at the resonant frequency of that mode. As stated earlier, an MXN uses a set of drivers to independently address all of the modes lying below a given cutoff frequency. The resonant frequency of each mode is determined by the physical parameters of the plate. The simplest case for determining resonant frequencies happens for simply supported boundary conditions, and are given by

$$\omega_{0_r} = \sqrt{\frac{D}{\rho h}}\Psi_r, \tag{13}$$

where Ψ_r is determined by the order m, n of the r-th mode as defined in Eq. (3). A more realistic formula for panel resonances when constructed of more practical means is given by (Mitchell, Hazell, 1987) and reflects fully clamped boundary conditions. This formula is a modified version of Eq. (13) and gives resonances as

$$\omega_{0_r} = \sqrt{\frac{D}{\rho h}}\Psi'_r, \tag{14}$$

where

$$\Psi'_r = \left(\frac{(m_r + \Delta m_r)\pi}{L_x}\right)^2 + \left(\frac{(n_r + \Delta n_r)\pi}{L_y}\right)^2 \tag{15}$$

and

$$\Delta m_r = \frac{1}{(\frac{n_r L_x}{m_r L_y})^2 + 2}, \qquad \Delta n_r = \frac{1}{(\frac{m_r L_y}{n_r L_x})^2 + 2}. \tag{16}$$

Equation (14) represents an ellipse in (m,n) space. An example of frequency contours is shown in Fig. 1 for a 1 mm thick aluminum plate measuring 113 mm by 189 mm in the x and y directions respectively. An $\mathbf{X}$ has been placed at the (m,n) locations for the eight modes with the lowest resonant frequencies.

A regularly spaced, rectangular array of actuators such as that used in (Anderson, Bocko, 2016a) addresses a set of modes defined by a rectangle in a graph of the type given in Fig. 1. In the case of eight drivers, or a 2×4 array, the modes $(1,1)$ through $(2,4)$ would be addressed. The scheme chosen in Fig. 1 does not address mode $(2,4)$ at 2300 Hz but instead addresses the $(1,5)$ mode because it has a slightly lower resonant frequency (2265 Hz).

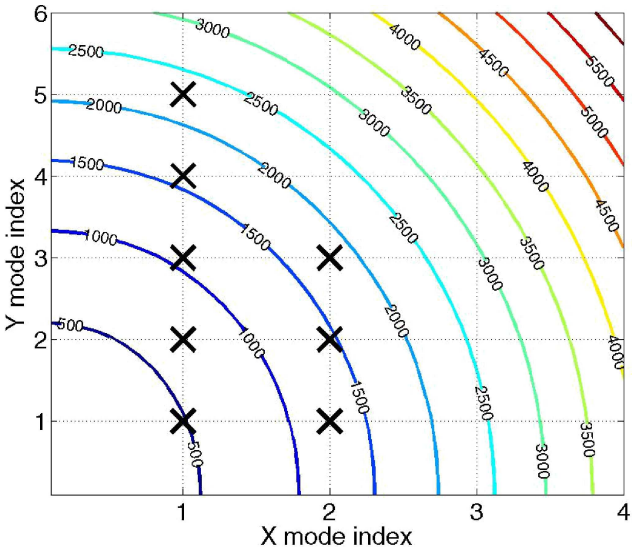

Fig. 1. Frequency contours for an aluminum plate with **X**s marking the indices of the eight lowest frequency modes.

2.2. Driver coupling efficiency

To determine how drivers should be placed on a panel, the term 'coupling efficiency' (CE) has been developed to represent the ratio of aggregate driver force to a modal force. For example, the individual driver forces necessary to induce a 1 N force on the first mode may be determined from Eq. (10). If the drivers do not couple well to this mode, the required driver forces will be very high, and the CE will be very small. In essence, the only way to achieve a CE value of 1 for a particular mode is to place drivers at only anti-nodes of that mode. In an MXN, however, the actuators are required to simultaneously drive multiple modes, each with its own set of nodes and anti-nodes. This suggests that placing drivers on the anti-nodes of a particular mode, though inducing a perfect coupling efficiency for that mode, may not be an ideal layout for an MXN, as this particular layout may result in weak coupling to other modes in the MXN bandwidth.

The matrix $\mathbf{G}^{-1}$ in Eq. (10) gives the individual driver force amplitudes necessary to generate each modal force, with terms β_{rl}, where r refers to the mode index and l refers to the driver index. The β terms represent the ratio of $\frac{F_{\text{in}}}{F_{\text{out}}}$ for a given mode at the location of each driver; a large β value indicates an inefficient force actuator position for driving a given mode.

$$\mathbf{G}^{-1} = \begin{bmatrix} \beta_{11} & \beta_{21} & \cdots & \beta_{N1} \\ \beta_{12} & \beta_{22} & \cdots & \beta_{N2} \\ \vdots & \vdots & \ddots & \vdots \\ \beta_{1N} & \beta_{2N} & \cdots & \beta_{NN} \end{bmatrix}. \tag{17}$$

The aggregate force ratio $\frac{F_{\text{in-total}}}{F_{\text{out-total}}}$ of the r-th mode relative to the driver array, Ω_r, is given by the sum of the β terms in the r-th column of Eq. (17). The CE will be defined as the inverse of this term, as given in Eqs. (18) and (19), and has a range between 0 and 1.

$$\begin{bmatrix} \Omega_1 & \Omega_2 & \cdots & \Omega_N \end{bmatrix} = \begin{bmatrix} 1 & 1 & \cdots & 1 \end{bmatrix} \mathbf{G}^{-1}, \tag{18}$$

$$CE_r = \frac{1}{\Omega_r}. \tag{19}$$

3. Point force driver locations

For a given MXN cutoff frequency, the layout of the actuator array should meet the following criteria. First, the drivers should have a low β value for all modes that lie below the MXN cutoff frequency. Second, each actuator should experience roughly the same β value with respect to each of the addressable modes. These criteria are used to ensure that the array is able to couple as evenly as possible to every mode shape in the controlled frequency region and that every driver does roughly the same amount of work in actuating each mode. For a specific mode, some drivers in the array will naturally see a lower driving point β value, but averaged over the full range of addressable modes the total β value seen by each driver should be about the same. To achieve this, the term given in Eq. (20) should be minimized, where β_{rl} refers to the elements of the matrix $\mathbf{G}^{-1}$. This optimization is carried out by varying the locations (x_d, y_d) of the N drivers to minimize ρ.

$$\rho = \sum_{r=1}^{N} \sum_{l=1}^{N} \beta_{rl}^2. \tag{20}$$

Since the optimization routine does not directly optimize the CE terms, coupling efficiency for the array may not be at its maximum value for a given modal set using this technique. However, for practical reasons, making sure that individual driver elements deliver the same amount of energy over the entire spatial bandwidth is given priority.

3.1. Point-force optimization results

Results in this section were obtained under the assumption that the drivers are massless point-force actuators, resulting in a $\mathbf{G}$ matrix with α terms from Eq. (6). The optimization routine was written in MATLAB, using the optimization toolbox. Results are shown in Fig. 2, including those for a regularly spaced, rectangular array layout. Table 1 gives the coupling efficiency metric for each mode addressed by the array, and shows that in each case the array couples to the selected modes with roughly the same efficiency. A key point to be inferred from this result is that the regularly spaced rectangular array is not optimally coupled to the N lowest frequency modes, and other, less regular, array layouts are optimal for various selections of the addressable modes.

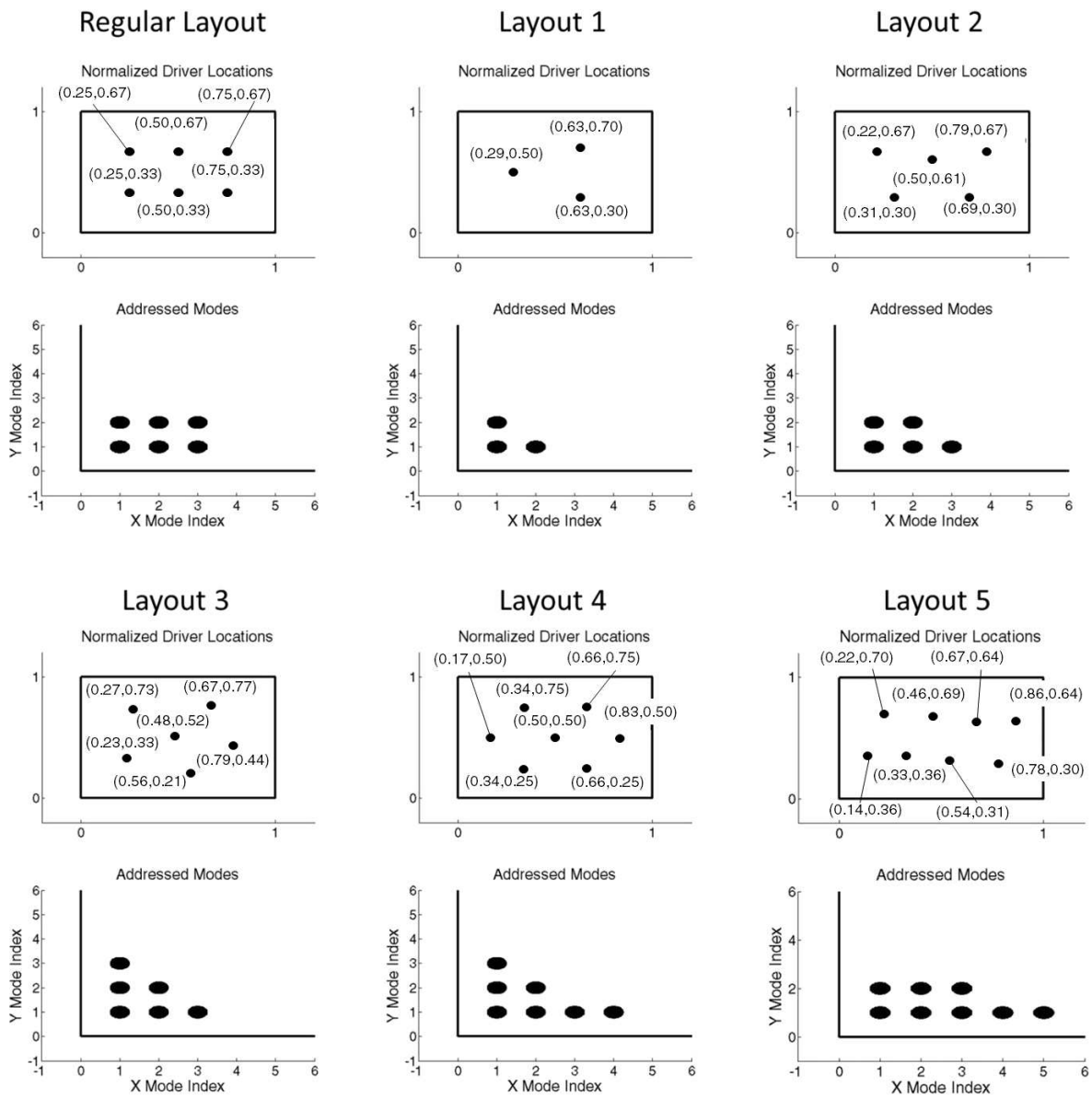

Fig. 2. Rectangular driver array shown with optimized layouts for 5 selected modal sets. The top frame shows driver locations (normalized) and the bottom frame shows which modes are addressed by the array.

Table 1. Coupling Efficiencies given by Eq. (19) for the addressed modes of each layout given in Fig. 2. Blank spaces represent modes that are not addressable by the array.

Mode Indices	Coupling Efficiency					
	Regular Layout	Layout 1	Layout 2	Layout 3	Layout 4	Layout 5
(1,1)	0.7131	0.7584	0.7159	0.6829	0.6742	0.6906
(2,1)	0.8607	0.8764	0.7994	0.7339	0.7148	0.7054
(3,1)	0.7131		0.7859	0.7516	0.9999	0.7669
(4,1)					0.7264	0.6856
(5,1)						0.7077
(1,2)	0.7260	0.7721	0.6812	0.7339	0.8754	0.6979
(2,2)	0.8763		0.8750	0.7805	0.8462	0.7202
(3,2)	0.7260					0.8096
(1,3)				0.7516	0.6842	

4. Piezoelectric actuator arrays

The optimal placement of piezoelectric actuators and sensors for controlling rigid structures has been studied extensively. The majority of the optimization methods were developed for the purpose of active noise control. Examples of these active control optimization routines, namely linear quadratic Gaussian (LQG) and linear quadratic regulator (LQR) control can be found in work by Fahroo and Wang (1997) and Devasia *et al.* (1993) for beams, and Hwang *et al.* (1997) for all-clamped plates. Early studies by Clark *et al.* (1993) showed that actuators centered on nodal lines of simply-supported plate modes are very poor exciters of these modes, and conversely, actuators located in the antinodal regions are very good exciters of the modes. This work provided experimental validation for the static model of a piezo-driven plate developed by Dimitriadis *et al.* (1991). Wang *et al.* (1994) and Li *et al.* (2001) investigated the optimal placement of rectangular piezoelectric actuators to control acoustic radiation from rectangular plates. The present method is related to work by Jia (1990) on Independent Modal Space Control (IMSC) of beams, which determined optimal actuator sizes and locations to give vibrational control over a given set of beam modes.

4.1. Background on piezo-driven plates

The analysis of Sec. 3 may be modified to treat the case of plate modal control via piezoelectric bending actuators. In addition to determining how the location of an actuator will couple to a given mode, the analysis also indicates how the size of the actuator relative to the spatial wavelength of a mode affects the coupling efficiency. Piezoelectric bending mode actuators polarized in the x, y plane expand or contract an amount proportional to their d_{31} and d_{32} expansion coefficients when a voltage is applied across the z dimension of the actuator. Assuming a perfect bond between the panel surface and the actuator, the expansion/contraction of the actuator off the neutral axis of the panel induces a series of bending moments at the actuator boundaries which cause the panel to bend. The frequency response of this displacement $w(x, y, \omega)$ for a plate excited by a single, rectangular actuator was found by Dimitriadis *et al.* (1991) and is given by

$$w(x,y,\omega) = \sum_{r=1}^{\infty} \frac{4DK^f \varepsilon \Gamma_r}{\rho L_x L_y h(\omega^2 - \omega_{0_r}^2)} \cdot [(\cos k_{m_r} x_1 - \cos k_{m_r} x_2) \cdot (\cos k_{n_r} x_1 - \cos k_{n_r} x_2)] H_r(x,y). \quad (21)$$

Here, ε is the unconstrained piezoelectric strain of the actuator, K^f is the actuator-plate material-geometric strain constant, k_{m_r} and k_{n_r} are wavenumbers of the r-th mode given by

$$k_{m_r} = \frac{m_r \pi}{L_x}, \quad (22)$$

$$k_{n_r} = \frac{n_r \pi}{L_y}, \quad (23)$$

and ω_{0_r} is defined for each mode as in Eq. (13). Γ_r is a modal stiffness constant defined as

$$\Gamma_r = \frac{k_{m_r}^2 + k_{n_r}^2}{k_{m_r} k_{n_r}}. \quad (24)$$

This term reflects the increasing stiffness of the plate when $m_r \neq n_r$. L_x, L_y, x_1, x_2, y_1, and y_2 are the plate and actuator dimensions shown in Fig. 3. This model assumes that the actuator dimensions (ℓ_x, ℓ_y) are much greater than the plate thickness (h) and that the actuator thickness is much smaller than the plate thickness. For simplicity, the actuator is assumed to induce identical strains in the x and y directions within the plane of the plate.

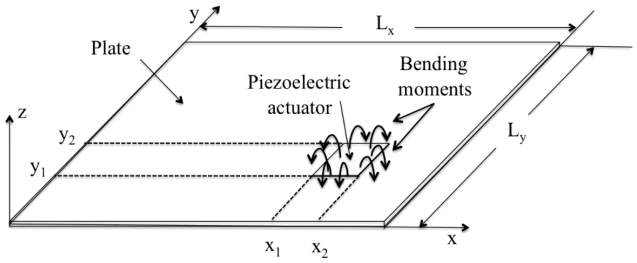

Fig. 3. Dimensions of a single piezo/plate system with induced bending moments.

The bending moments shown in Eq. (21) can be simplified and represented as an equivalent point force acting at location (a, b), the center of the piezoelectric actuator as shown in Fig. 4, where

$$\ell_x = |x_2 - x_1|, \quad (25)$$

$$\ell_y = |y_2 - y_1|. \quad (26)$$

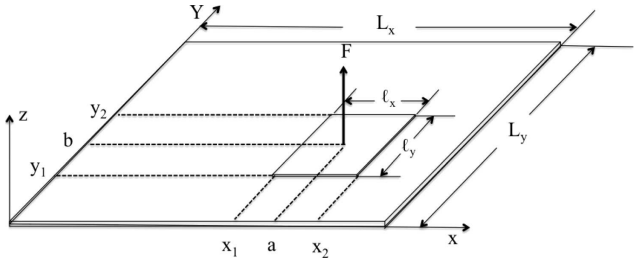

Fig. 4. Equivalent point force of bending moment system.

The magnitude of the point force can be written as

$$F = \sum_{r=1}^{\infty} F_r = \sum_{r=1}^{\infty} 4DK^f \varepsilon \Gamma_r \alpha_r \left(\frac{\ell_x}{2}, \frac{\ell_y}{2}\right) \tag{27}$$

which implies that $w(x, y, \omega)$ for the piezoelectric patch shown in Fig. 4 can be written as

$$w(x, y, \omega) = \sum_{r=1}^{\infty} \frac{4F_r \alpha_r(a, b) H_r(x, y)}{\rho L_x L_y h(\omega^2 - \omega_{0_r}^2)}. \tag{28}$$

This will serve as the framework for determining optimal piezoelectric array layouts.

4.2. Piezoelectric driver locations

Clark *et al.* (1991) demonstrated that the response of a structure excited by multiple piezoelectric actuators can be modeled as a linear combination of single actuator responses. This means that the method for point force driver optimization presented in Sec. 3 can be extended for piezoelectric actuators without significant modification.

It is important to note that the magnitude of the force induced by a piezoelectric actuator on a given mode will depend upon the relative dimensions of the actuator and the wavelength of the mode. Small actuators for example, are less effective at driving low-frequency modes with spatial wavelengths much greater than the actuator dimensions. Conversely, when the curvature of the actuator matches the curvature of the mode, the mode can be effectively excited with a relatively small input voltage. The matrix **G** presented in Eq. (8) must be modified to account for the modally varying point force in Eq. (27). The result is the matrix **K**, where

$$\mathbf{K} = \begin{bmatrix} \gamma_1(x_1, y_1) & \gamma_1(x_2, y_2) & \cdots & \gamma_1(x_N, y_N) \\ \gamma_2(x_1, y_1) & \gamma_2(x_2, y_2) & \cdots & \gamma_2(x_N, y_N) \\ \vdots & \vdots & \ddots & \vdots \\ \gamma_N(x_1, y_1) & \gamma_N(x_2, y_2) & \cdots & \gamma_N(x_N, y_N) \end{bmatrix} \tag{29}$$

with the elements $\gamma_r(x_i, y_i)$ given by

$$\gamma_r(x_i, y_i) = \Gamma_r \alpha_r \left(\frac{\ell_{x_i}}{2}, \frac{\ell_{y_i}}{2}\right) \alpha_r(x_i, y_i). \tag{30}$$

For simplicity, the factors D, K^f and ε from Eq. (27) have been factored out of Eq. (30), as these are not functions of either the mode being driven or the actuator location and will not affect the optimized driver position as long as we assume that all actuators are made of the same piezoelectric material. If the array employs a combination of piezoelectric materials the appropriate material factors must be added to the rows of **K** in Eq. (30). The actuator locations can then be inferred using the method described in Sec. 3.

4.3. Simulated examples

The following section presents several examples of piezoelectric patch array configurations for exciting different sets of modes. To simplify the analysis, the actuators are assumed to be square, and the dimensions of each patch are presented as normalized fractions of the panel dimensions. For the sake of brevity, this analysis is only concerned with actuators that are all the same size. It should be noted however, that the voltage efficiency of the driving array can be significantly improved for specific modes or combinations of modes by tailoring the actuator sizes to couple effectively to the specified modes within the given set. The array layouts for two different sized actuators are presented in Figs. 5 and 6, which address the same sets of modes considered in Fig. 2.

The layout determined for an array of identically sized piezoelectric actuators is similar to that found for an array of point force actuators; however, the center positions of the piezoelectric actuators are shifted slightly from the corresponding positions of point force actuators toward the center of the panel. This shift is due to inclusion of the $(1, 1)$ mode which is more effectively driven by a given piezoelectric actuator when it is closer to the center of the panel where the bending curvature of the $(1, 1)$ mode is greatest. The solutions to the optimization problem also assume that no two actuators can overlap, although this constraint could be relaxed.

One might expect the change in actuator location to become more significant as the actuator dimensions are decreased relative to the dimensions of the panel. Although some further shifts in the optimal driver locations are observed, the magnitude of the shifts are relatively small and the general layout of the driver array remains consistent. Since the layouts are similar for arrays with different actuator sizes, the coupling efficiencies of the arrays will remain similar as well. The effect of changing the actuator size is reflected in the voltage efficiency (*VE*) for a given array, where different size actuators require different input voltages to produce the same force on a given mode. *VE* is defined as

$$VE_r = CE_r * \Gamma_r \alpha_r \left(\frac{\ell_{x_i}}{2}, \frac{\ell_{y_i}}{2}\right) \tag{31}$$

to account for the actuator size relative to the r-th mode. The CE and VE values for each mode set are shown in Tables 2 and 3.

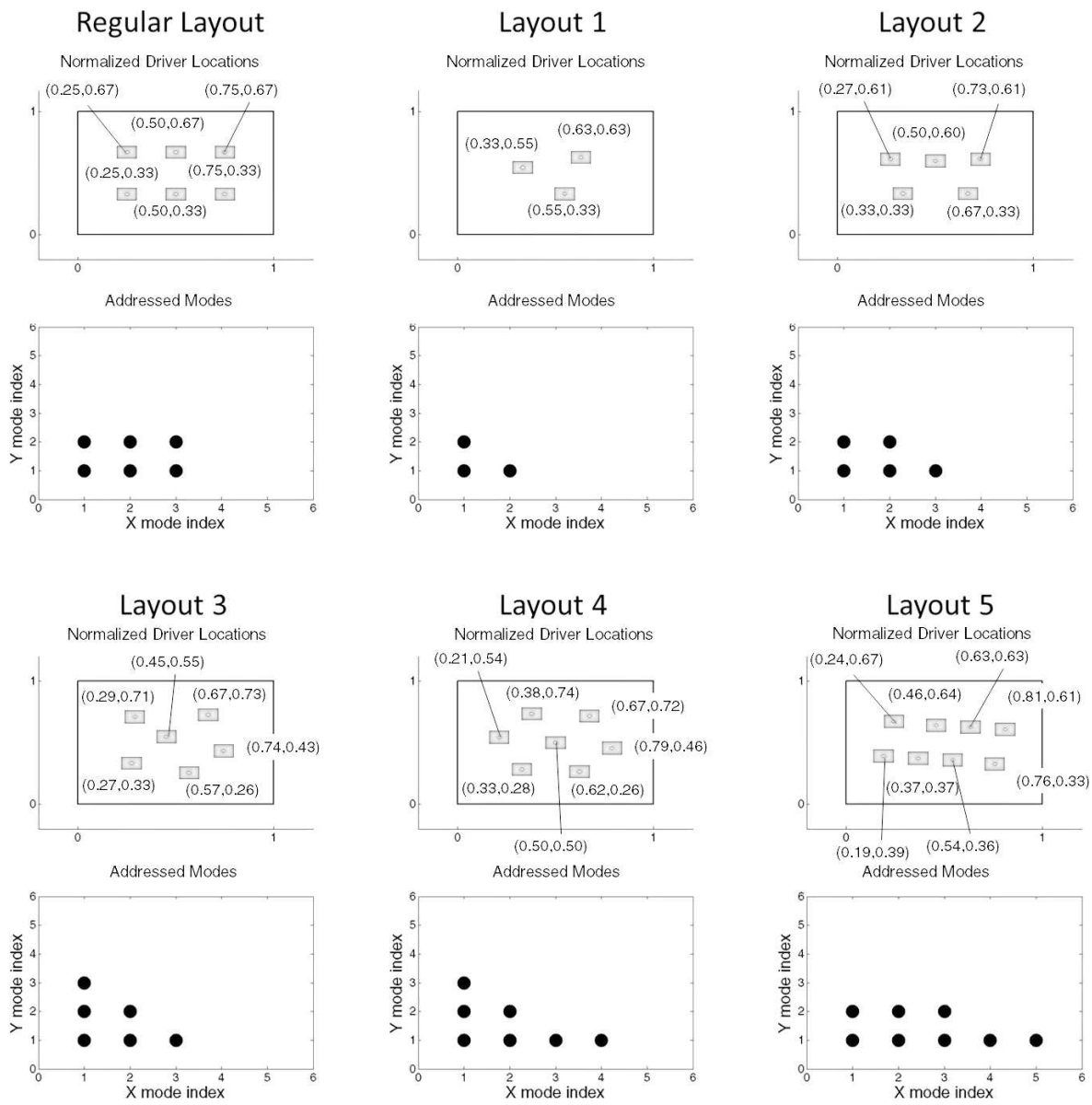

Fig. 5. The rectangular actuator array and the optimized layouts for five other selected modal sets are shown. Actuator dimensions are assumed to be (1/10)-th of the panel dimensions. The upper frames show the driver locations (normalized) and the lower frames indicate the modes that are addressed by the array.

Table 2. Coupling efficiency (CE) and voltage efficiency (VE) given by Eqs. (19) and (31) for the addressed modes of each layout given in Fig. 5. Blank spaces represent modes that are not addressable by the array.

Mode Indices	Regular Layout		Layout 1		Layout 2		Layout 3		Layout 4		Layout 5	
	CE	VE	CE	VE	CE	VE	CE	VE	CE	VE	CE	VE
(1,1)	0.713	0.035	0.851	0.041	0.775	0.038	0.719	0.035	0.707	0.035	0.740	0.036
(2,1)	0.861	0.104	0.705	0.086	0.844	0.103	0.749	0.090	0.829	0.099	0.774	0.092
(3,1)	0.713	0.169			0.689	0.166	0.608	0.142	0.802	0.194	0.694	0.167
(4,1)									0.602	0.239	0.641	0.250
(5,1)											0.465	0.262
(1,2)	0.726	0.088	0.705	0.086	0.641	0.077	0.749	0.090	0.820	0.100	0.630	0.076
(2,2)	0.876	0.167			0.705	0.135	0.753	0.144	0.697	0.133	0.626	0.119
(3,2)	0.726	0.221									0.656	0.202
(1,3)							0.608	0.142	0.639	0.156		

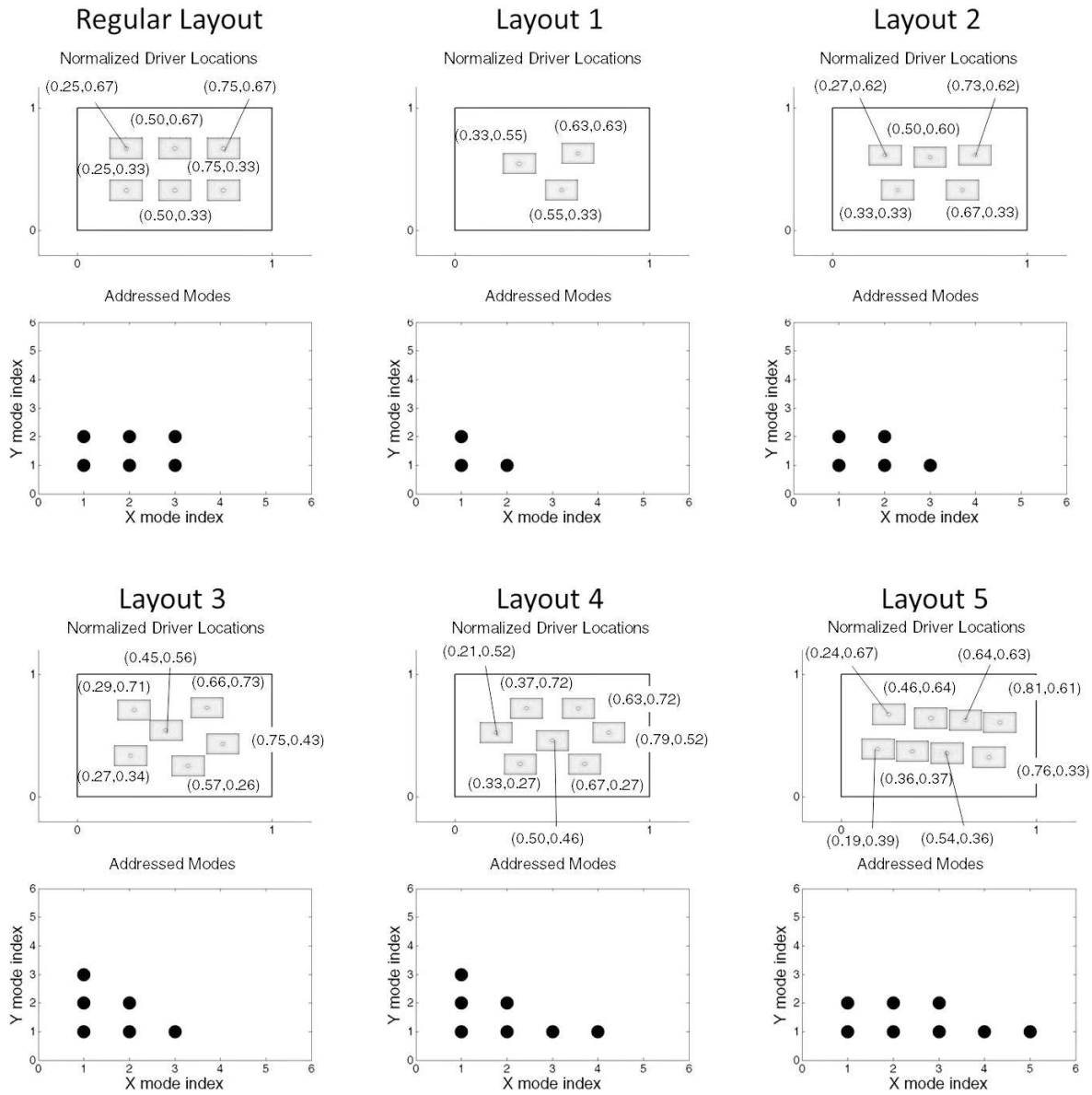

Fig. 6. The rectangular actuator array and the optimized layouts for five other selected modal sets are shown. Actuator dimensions are assumed to be (1/6)-th of the panel dimensions. The upper frames show the driver locations (normalized) and the lower frames indicate the modes that are addressed by the array.

Table 3. Coupling efficiency (CE) and voltage efficiency (VE) measurements given by Eqs. (19) and (31) for the addressed modes of each layout given in Fig. 6. Blank spaces represent modes that are not addressable by the array.

Mode Indices	Regular Layout		Layout 1		Layout 2		Layout 3		Layout 4		Layout 5	
	CE	VE	CE	VE	CE	VE	CE	VE	CE	VE	CE	VE
(1,1)	0.713	0.096	0.849	0.114	0.773	0.103	0.718	0.096	0.707	0.095	0.738	0.099
(2,1)	0.861	0.279	0.709	0.231	0.843	0.273	0.750	0.248	0.826	0.266	0.772	0.249
(3,1)	0.713	0.435			0.691	0.419	0.617	0.379	0.816	0.507	0.697	0.424
(4,1)									0.622	0.595	0.644	0.610
(5,1)											0.485	0.638
(1,2)	0.726	0.235	0.709	0.231	0.644	0.210	0.750	0.238	0.806	0.254	0.635	0.204
(2,2)	0.876	0.438			0.712	0.364	0.753	0.380	0.759	0.374	0.633	0.322
(3,2)	0.726	0.556									0.664	0.507
(1,3)							0.617	0.372	0.614	0.371		

5. Experiments

To evaluate the ability of an optimized array to address the specified modes, a panel using an array of eight dynamic force actuators was constructed, using point-force layout 5 from Subsec. 3.1. The plate is a 1 mm thick aluminum panel with dimensions 113 mm by 189 mm, matching the analysis from Subsec. 2.1. It is epoxy bonded at its edges to an acrylic frame. A picture of the prototype is shown in Fig. 7.

In the experiments, we sought to validate that the array was able to independently address the eight panel modes with the lowest resonant frequencies that match the analysis in Fig. 1. The key feature that we sought to demonstrate is that it is possible to drive each addressable mode independently without exciting any of the other addressable modes.

The drivers used were Dayton Audio DAEX9CT-4 0.5W moving-coil actuators, each powered by an independent Texas Instruments TPA3110D2 class-D amplifier channel. It is worth noting that a large array of drivers with non-negligible mass and their own resonant frequencies will have a noticeable effect on the resonant properties of the panel. When the drivers were placed on the plate, they showed an actuator resonance near 180 Hz, giving each plate mode a second resonance near this frequency.

Each mode was driven independently of the other modes by setting the respective mode force amplitude to unity and the remaining mode forces to 0 in Eq. (10). Driver force amplitudes are given by the **D** array, which are simply proportional to the voltage across each moving-coil driver. The driver scaling amplitudes are given in Table 4. Voltage scaling was performed using MAX MSP software. The vibrational characteristics of the panel up to 4 kHz were determined using a Polytec PSV-500 scanning laser vibrometer. The results are shown in Fig. 8.

In each frame of Fig. 8, the velocity clearly shows a peak near the resonant frequency of the mode being addressed. There also are spectral features in each figure below 200 Hz, which arise from the resonant behavior of the driver elements themselves. In the frequency scan when the $(1,4)$ mode is addressed, spillover to the $(2,5)$ mode appears, and in the scan for the $(2,3)$ mode, spillover to the $(1,6)$ mode appears. Interestingly, the $(1,5)$ mode scan has spillover to the $(2,4)$ mode, which has only a slightly higher resonant frequency, distorting the appearance of the $(1,5)$ mode.

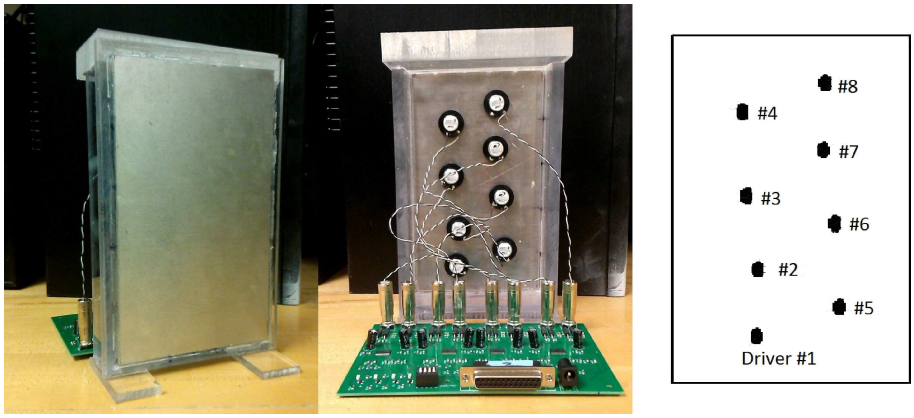

Fig. 7. Prototype loudspeaker with 8 drivers and amplifier board. The driver positions are indexed on the right-side diagram.

Table 4. Driver scaling amplitudes for actuating individual modes using the experimental setup of Fig. 7.

Mode Under Drive	Driver Scaling Amplitudes							
	Driver #1	#2	#3	#4	#5	#6	#7	#8
(1,1)	0.0827	0.2329	0.2495	0.1591	0.1591	0.2495	0.2329	0.0827
(1,2)	0.1613	0.2376	−0.0766	−0.2308	0.2308	0.0766	−0.2376	−0.1613
(1,3)	0.2351	−0.0191	−0.2101	0.1876	0.1876	−0.2101	−0.0191	0.2351
(1,4)	0.2533	−0.2577	0.1423	−0.0717	0.0717	−0.1423	0.2577	−0.2533
(1,5)	0.2253	−0.2454	0.1760	−0.0778	−0.0778	0.1760	−0.2454	0.2253
(2,1)	0.0925	0.1727	0.2633	0.1853	−0.1853	−0.2633	−0.1727	−0.0925
(2,2)	0.1637	0.1797	−0.0688	−0.2842	−0.2842	−0.0688	0.1797	0.1637
(2,3)	0.1770	0.0089	−0.2137	0.2195	−0.2195	0.2137	−0.0089	−0.1770

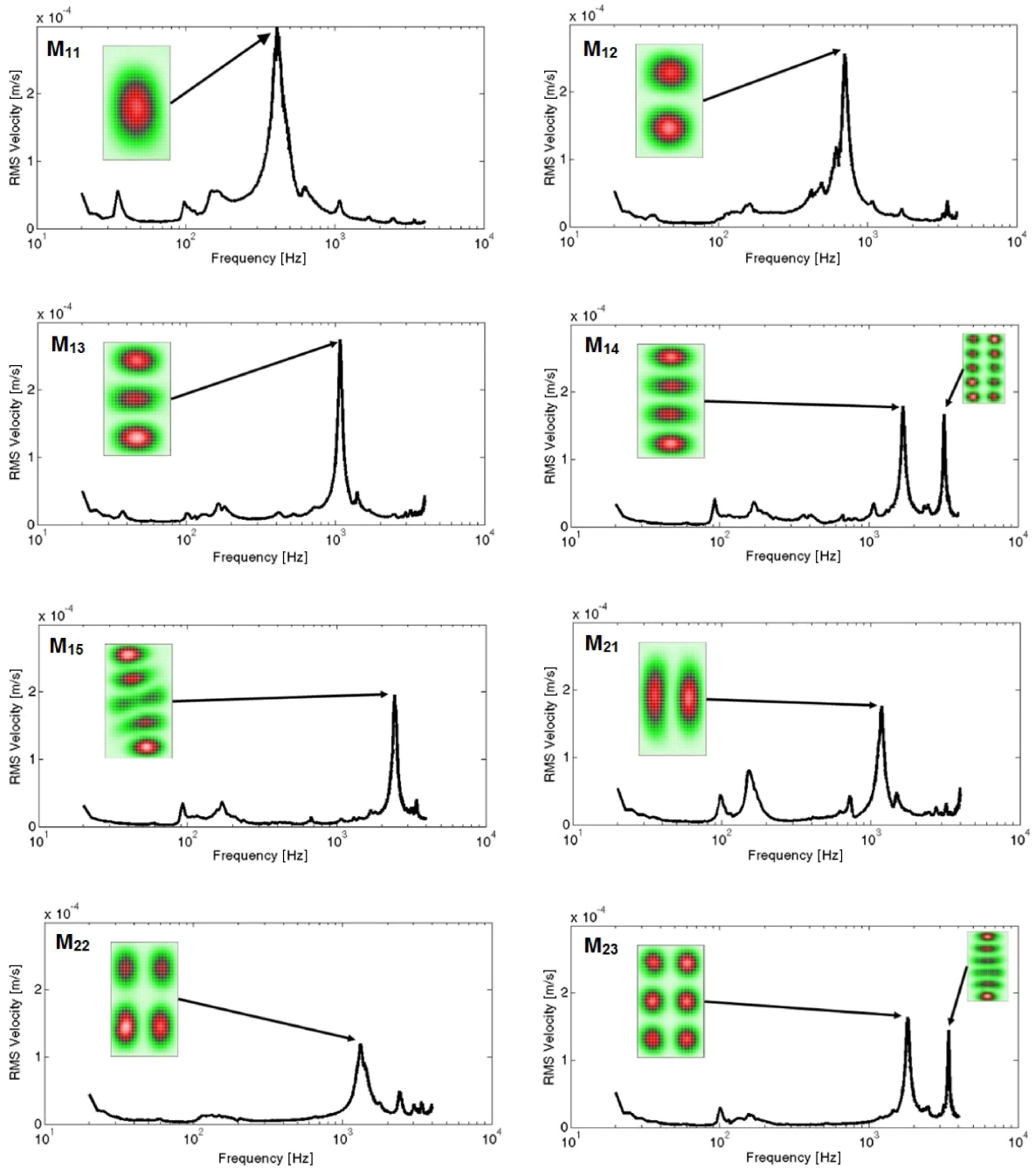

Fig. 8. (8 frames) Scans of each mode, driven independently by the array. In each scan it can be seen that in the frequency range of interest, no vibrational modes are apparent other than the driven mode. Vibrometer scan images of the mode shape at its resonant frequency are given for each case, as well as easily identifiable 'spillover' (out of band) modes.

6. Conclusion

A method was described for finding the optimal force actuator locations for controlling a selected set of bending modes of a flat panel. In the applications of specific interest in this paper (flat panel loudspeakers) it is important to be able to exert independent control over each of the modes in a low-pass frequency band. The geometry of the modes in such a set may vary greatly, which implies that the layout of the actuator array that would be most effective at driving each mode is unique, since a mode is driven most effectively by actuators near a mode's antinodes. An optimization method was employed to determine the actuator locations that are able to drive every mode in a selected set as equally as possible and to spread the work evenly among the force actuators in the array. Simulations show that either point-force actuators or piezoelectric bending actuators have global optima that give large coupling efficiency between the actuators and modes.

Experimental results on an aluminum panel show that all modes lying below a given cutoff frequency can be addressed independently by the optimally determined actuator array. Although the methods described here were developed for the control of plates for flat-panel loudspeakers, these techniques should also prove useful to many other problems of structural vibration control.

References

1. Anderson D., Bocko M.F. (2015), *A model for the impulse response of distributed-mode loudspeakers and multi-actuator panels*, 139th Convention of the AES.
2. Anderson D., Bocko M.F. (2016a), *Modal crossover networks for flat-panel loudspeakers*, J. Audio Eng. Soc., **90**, 1, 346–357.
3. Anderson D., Bocko M.F. (2016b), *Measures of vibrational localization on point-driven flat-panel loudspeakers*, 171st Meeting of the Acoustical Society of America.
4. Bank G., Harris N. (1998), *The distributed mode loudspeaker-theory and practice*, AES 13th UK Conference: Microphones & Loudspeakers.
5. Clark R.L., Fuller C.R., Wicks A. (1991), *Characterization of multiple piezoelectric actuators for structural excitation*, J. Acoust. Soc. Am., **90**, 1, 346–357.
6. Clark R.L., Flemming M.R., Fuller C.R. (1993), *Piezoelectric actuators for distributed vibration excitation of thin plates: a comparison between theory experiment*, ASME J. Vib. Acoust., **115**, 3, 332–339.
7. Demetriou M.A. (2000), *A numerical algorithm for the optimal placement of actuators and sensors for flexible structures*, Proceedings of the American Control Conference.
8. Devasia D., Meressi T., Paden B., Bayo E. (1993), *Piezoelectric actuator design for vibrations suppression: placement and sizing*, J. Guid. Control Dynam., **16**, 5, 859–864.
9. Dimitriadis E.K., Fuller C.R., Rogers C.A. (1991), *Piezoelectric actuators for distributed vibration excitation of thin plates*, ASME J. Vib. Acoust., **113**, 1, 100–107.
10. Fahroo F., Wang Y. (1997), *Optimal location of piezoceramic actuators for vibration suppression of a flexible structure*, Proceedings of the 36th Conference on Decision and Control.
11. Fuller C., Elliott S., Nelson P. (1996), *Active Control of Vibration*, Associated Press.
12. Hwang J.K., Choi C.-H., Song C.K., Lee J.M. (1997), *Robust LQG control of an all-clamped thin plate with piezoelectric actuators/sensors*, IEEE/ASME Transactions on Mechatronics, **2**, 3, 205–212.
13. Jia J. (1990), *Optimization of Piezoelectric Actuator Systems for Vibration Control of Flexible Structures*, PhD thesis, Virginia Polytechnic Institute and State University.
14. Li L.X., Shen Y.P., Gao F. (2001), *The optimal design of piezoelectric actuators for acoustic control*, Smart Materials and Structures, **10**, 2, 421–426.
15. Mitchell A.K., Hazell C.R. (1987), *A simple frequency formula for clamped rectangular plates*, J. Sound and Vib., **118**, 2, 271–281.
16. Porter B., Crossley R. (1972), *Modal Control: Theory and Applications*, Taylor and Francis.
17. Rabbiolo G., Bernhard R., Milner F. (2004), *Definition of a high-frequency threshold for plates and acoustical spaces*, J. Sound and Vib., **277**, 4–5, 647–667.
18. Wang B.T., Burdisso R.A., Fuller C.R. (1994), *Optimal placement of piezoelectric actuators for active structural acoustic control*, Journal of Intelligent Material Systems and Structures, **5**, 1, 67–77.